Insights from modeling metabolism and amoeboid cell motility in the immune system

Steijn, L. van

Chapter 5

A novel function of TLR2 and MyD88 in the regulation of leukocyte cell migration behavior during wounding in zebrafish larvae

Wanbin Hu, Leonie van Steijn, Chen Li, Fons J. Verbeek, Lu Cao, Roeland M.H. Merks, Herman P. Spaink *

Abstract

Toll-like receptor (TLR) signaling via myeloid differentiation factor 88 protein (MyD88) has been indicated to be involved in the response to wounding. It remains unknown whether the putative role of MyD88 in wounding responses is due to a control of leukocyte cell migration. The aim of this study was to explore *in vivo* whether TLR2 and MyD88 are involved in modulating neutrophil and macrophage cell migration behavior upon zebrafish larval tail wounding. Live cell imaging of tail-wounded larvae was performed in *tlr2* and *myd88* mutants and their corresponding wild type siblings. In order to visualize cell migration following tissue damage, we constructed double transgenic lines with fluorescent markers for macrophages and neutrophils in all mutant and sibling zebrafish lines. Three days post fertilization (dpf), tail-wounded larvae were studied using confocal laser scanning microscopy (CLSM) to quantify the number of recruited cells at the wounding area. We found that in both *tlr2*$^{-/-}$ and *myd88*$^{-/-}$ groups the recruited neutrophil and macrophage numbers are decreased compared to their wild type sibling controls. Through analyses of neutrophil and macrophage migration patterns, we demonstrated that both *tlr2* and *myd88* control the migration direction of distant neutrophils upon wounding. Furthermore, in both the *tlr2* and the *myd88* mutants,

*Modified from Wanbin Hu et al. "A novel function of TLR2 and MyD88 in the regulation of leukocyte cell migration behavior during wounding in zebrafish larvae". *Frontiers in Cell and Developmental Biology* 9 (2021), 210

macrophages migrated more slowly towards the wound edge. Taken together, our findings show that *tlr2* and *myd88* are involved in responses to tail wounding by regulating the migratory behavior of leukocytes *in vivo*.

5.1 Introduction

Acute inflammation is characterized by the directed migration of leukocytes, which can be triggered by tissue damage [212, 213]. The function of directed leukocyte migration is to eliminate cell debris and invading pathogens, with the aim of maintaining homeostasis upon tissue damage [214]. Neutrophils and macrophages are the two crucial immune cells that engage in this process [213, 215]. Neutrophils are the first cells to rapidly respond to the site of injury, and produce cytokines and chemokines to mediate the recruitment of other cells [216, 215]. However, persisting neutrophil recruitment can release toxic granule contents to further damage tissue, and thereby is a hallmark of chronic inflammatory disease [217, 214, 218]. In comparison, distant macrophages move slower and accumulate later at the wounded area and are considered to play a role in eliminating the debris of apoptotic cells and assist in regeneration of wounded tissue [219, 213, 215, 220]. Leukocyte migration must be tightly regulated to avoid negative effects on tissue repair or further damage. Despite myriad studies on leukocyte migration in response to wounding, the underlying mechanisms are not yet completely understood [221].

Neutrophils and macrophages depend on membrane-localized pattern recognition receptors (PRRs) to sense invading microbes and associated tissue damage [222]. PRRs play a crucial role to recognize pathogen associated molecular patterns (PAMPs) of invading microbes in open wounds and damage associated molecular patterns (DAMPs) released by lysing cells [223, 224]. Toll-like receptors (TLRs) are prominent recognition factors for PAMPs and DAMPs to regulate inflammatory responses [225, 226]. Extensive studies have demonstrated that cellular distribution is different for each TLR. TLRs recognize different classes of PAMPs and trigger the production of cytokines and chemokines during infection. Two typical examples are TLR2, which senses bacterial lipoproteins [227] , and TLR4, which recognizes bacterial lipopolysaccharide (LPS) [228]. Accumulating evidence shows that high-mobility group box 1 protein (HMGB1), which is the best well known endogenous danger signal, activates inflammation by forming complexes with other DAMPs (such as single-stranded DNA, nucleosomes and LPS) to be recognized by IL-1R as well as TLR2, TLR4

and TLR9 to induce inflammatory responses [229, 230, 213]. After interacting with these PAMPs and DAMPs, TLRs initiate downstream signaling cascades that ultimately result in producing cytokines and chemokines. Importantly, the activation of downstream signaling pathway by HMGB1 has been shown to be dependent on the TLR down-stream signaling mediated by myeloid differentiation factor 88 protein (MyD88) [213, 231].

TLR2 is one of the best known PRRs and acts as a heterodimer with TLR1 or TLR6 to recognize gram positive bacteria including mycobacteria, presumably based on the specific binding to their cell wall components, such as glycolipids and glycoproteins [227, 232]. TLR2 is expressed and activated after tissue injury even in the absence of infections, like in acute ischemic injury as well as in acute liver and kidney injury [233, 234, 235, 236]. In the study of Mojumdar *et al.* (2016), it was shown that macrophage infiltration was reduced into normal muscle following acute injury in TLR2 deficiency mice [237]. In addition, Kim et al. demonstrated that TLR2 contributes to macrophage infiltration in the dorsal root ganglia after peripheral nerve injury in mice [238]. Such injury-induced TLR2 expression and activation has therefore been hypothesized to be important for human health [239, 240, 236]. Following ischemic injury in mice, TLR2 activation promotes cell permeability, lymphocyte invasion and endothelial cell migration and mediates the release of TNF-α and IL-6 [235]. TLR2-deficient mice have a defective ability to recruit neutrophils to an injured liver and fail to induce the neutrophil chemokine CXCL-2 [236]. Additionally, TLR2 contributes to chronic liver disease in a mouse model by mediating MAPK and NF-$\varkappa$B signaling pathways [241]. However, there is little knowledge of the function of Toll-like receptor signaling in cell migration of myeloid cells to epithelial wounding sites [242].

MyD88 is an essential adaptor protein for all TLRs, except TLR3 [243, 244]. MyD88 is responsible for activating downstream signaling through binding to the TIR domain of TLRs [243, 244]. A few studies have shown changes in MyD88 expression after tissue injury. Similar to *Tlr2*, the gene expression of *Myd88* is upregulated following ischemic injury in mice [245]. Moreover, the expression of *Myd88* and *Tlr2* is significantly increased in diabetic wounded mice [246]. In addition, indirect evidence indicates that Myd88 is involved in the modulation of wound healing [247, 248], but the underlying mechanism is still unclear. Although TLR signaling is important for chemokine production, little is known about the role of MyD88 in leukocyte migratory responses to tissue injuries in the absence of pathogenic infections.

In this paper we use zebrafish larvae as a model for studying leukocyte cell migration after tail wounding. The zebrafish model has become an

important vertebrate model for studying human diseases. The small size and transparency of their larvae are useful characteristics for the screening and imaging of transgenic reporter lines [249]. Zebrafish larvae are a popular model for studying functions involved in wound repair [250, 251, 252, 253, 254, 255]. The availability of mutants in Toll-like receptor signaling genes *tlr2* and *myd88* make it possible to study their roles in leukocyte migratory behavior upon tail wounding in zebrafish [256, 257, 258, 252, 255]. Tlr2 and Myd88 show a highly conserved structure in mammals and zebrafish [259]. In a previous study, we demonstrated the conserved role of *tlr2* in zebrafish as a PRR to recognize the mammalian TLR2 ligand Pam3CSK4, and identified a set of genes that are specifically expressed genes by activation of the downstream pathway of zebrafish *tlr2* [260].

In the present study, live fluorescent imaging was used to investigate the effect of the *tlr2* mutation and the *myd88* mutation on leukocyte migration upon tail wounding. We found reduced numbers of recruited neutrophils and macrophages at the wounding area in both *tlr2* mutants and *myd88* mutants, compared to their sibling controls. Leukocyte migration of the *tlr2* and *myd88* mutations upon wounding was analyzed using quantitative analyses of cell migration tracks. Our results demonstrate that the *tlr2* and the *myd88* mutations affect distant neutrophil migration upon wounding by negatively affecting their directional persistence, but not their migration speed. Not only the directional persistence of distant macrophage was significantly decreased in the *tlr2* and the *myd88* mutants, but also their migration speed. This study shows for the first time that TLR signaling is directly involved in controlling behavior of cell migration of neutrophils and macrophages during wounding, stimulating further studies also in other model systems.

5.2 Materials and methods

5.2.1 Zebrafish maintenance and strain construction

All animal experiments described in this study were performed at the University of Leiden according to standard protocols (zfin.org) and adhered to the international guidelines specified by the EU Animal Protection Directive 2010/63/EU. The culture of adult fish was approved by the local animal welfare committee (DEC) of the university (License number: protocol 14,198). No adult zebrafish were sacrificed for this study. All experiments were done on 3 days post fertilization (dpf) fish, therefore prior to the free-feeding stage and did not fall under animal experimentation law according to the EU Animal Protection Directive 2010/63/EU. Eggs

and larvae were grown at 28.5°C in egg water (60 g/ml Instant Ocean sea salts). For living imaging and tail wounding experiments, 3 dpf larvae were anesthetized with egg water containing 0.02% buffered 3-aminobenzoic acid ethyl ester (Tricaine, Sigma-Aldrich, the Netherlands).

The *tlr2*^{sa19423} mutant and *myd88*^{hu3568} mutant lines were identified by the sequencing of an ENU-mutagenized zebrafish library [257, 258]. Both homozygous mutants were outcrossed with the double transgenic line *Tg (mpeg1:mCherry-F);TgBAC (mpx: EGFP)* [250, 261]. Subsequently, their heterozygous offspring with both positive GFP and mCherry fluorescence were incrossed to produce the homozygous mutants and wild type siblings. In the present study, the double transgenic lines were used for the quantification of cell numbers, recruitment assay upon wounding and leukocyte living imaging experiment.

To investigate the effect of the *tlr2* and the *myd88* mutations on leukocyte development, double fluorescent lines *tlr2*$^{+/+}$ *Tg (mpeg1:mCherry-F);TgBAC (mpx: EGFP)*, *tlr2*$^{-/-}$ *Tg (mpeg1:mCherry-F);TgBAC (mpx: EGFP)*, *myd88*$^{+/+}$ *Tg (mpeg1:mCherry-F);TgBAC (mpx: EGFP)*, *myd88*$^{-/-}$ *Tg (mpeg1:mCherry-F);TgBAC (mpx: EGFP)* were used.

5.2.2 Tail wounding

In the present study, a caudal fin wounding model was applied as previously described [250, 262, 252]. 3 dpf *tlr2* zebrafish larvae were anesthetized with egg water containing 0.02% tricaine (Sigma Aldrich). Subsequently, the caudal fins of larvae were wounded by using a 1 mm sterile sapphire blade scalpel (World Precision Instruments) on a 2% agarose covered petridish. To avoid damaging the notochord and other tissues of zebrafish larvae, all of the wounding experiments were performed under a MZ16FA Fluorescence Stereo Microscope (Leica Microsystems, Wetzlar Germany) equipped with a DFC420C color camera (Leica Microsystems). After the wounding, the egg water with 0.02% tricaine was changed with untreated egg water. Wounded larvae were put back into an incubator at 28.5°C. Subsequently, the wounded larvae were collected or fixed for follow up experiments.

5.2.3 Imaging and quantification

For the quantification of the recruited cell number upon wounding, the double transgenic *tlr2* and *myd88* larvae were wounded with the method described before. 1, 2, 4 and 6 hour post wounding (hpw), larvae were collected and fixed with 4% paraformaldehyde (PFA) in PBS overnight

at 4°C and washed with PBS the next day. The wounded tail area of fixed samples from each group were imaged by using a Leica MZ16FA fluorescence stereo microscope equipped with a DFC420C color camera. Cells localized within an area of 200 µm from the wounding edge toward the body trunk were counted as recruited cells. Analysis was performed by combining three independent experiments.

For detailed cell migration behavior analyses, larvae (3 dpf) were mounted into 1% low melting point agarose (Sigma Aldrich) with 0.02% tricaine and imaged under a Leica TCS SP8 confocal microscope (Leica Microsystems) with a 10× objective (N.A. 0.40). Data were saved as maximum projection images for further cell counting. The number of neutrophils and macrophages in the tail region were manually quantified.

5.2.4 Live imaging

All time-lapse imaging was performed on 3 dpf larvae. Larvae for each condition (unchallenged/ wounded) were mounted in the method described before and visualized in the CLSM with 1 min time interval for 2 h image capture using a 20× objective (N.A. 0.75). For the cell tracking analysis, all time-lapse images were saved as maximum projection images.

We first defined the role of *tlr2* and *myd88* in leukocyte migration under the unchallenged condition. The caudal hematopoietic tissue (CHT) of double transgenic lines was imaged using the CLSM with unchallenged condition. To investigate the effect of the *tlr2* and *myd88* mutations on leukocyte migration upon wounding, the double transgenic line *Tg (mpeg1:mCherry-F);TgBAC (mpx: EGFP)* larvae in the *tlr2*, *myd88* mutant or their wild type background were wounded and performed for real time imaging from 1 hpw to 3 hpw.

5.2.5 Cell tracking and its quantification

The cell tracking of macrophages and neutrophils was performed manually by using a manual tracking plug-in from Fiji [263, 264]. To analyze the behavior of leukocyte tracks more accurately, we defined categories of distant and local resident cells. Cells localized further than 200 µm from the cut edge towards the trunk were categorized as distant cells. Cell localized within a distance of up to 200 µm from the cut toward to the trunk were categorized as local resident cells.

The distance to the wound, mean speed, net displacement, meandering index (M.I.), mean square displacement (MSD), cell diffusivity (D), velocity in anteroposterior direction (V_{AP}) and V_{AP} over time were calculated in

different groups by manual tracking data. The calculation and explanation of the parameters are shown in Figure 5.1. The distance to the wound is defined as the shortest Euclidean distance to the manually traced wound edge (Figure 5.1A). For the velocity in the anteroposterior direction, tracks were rotated such that the spines of the larvae were aligned (Figure 5.1B). Then, for each cell the average velocity in the anteroposterior axis was calculated. For V_{AP} over time, the V_{AP} of all cells within a group was averaged over three consecutive time frames. Net displacement, total displacement, meandering index and mean speed are shown in Figure 5.1C and Table 5.1 (Eqs. 5.1-5.4). The net displacement is the distance of the cell between the first and final time frame (Figure 5.1C), i.e., the Euclidian distance traveled being: $d_{\text{net}} = d\left(p_i, p_N\right)$ (Table 5.1. Eq. 5.1). The total displacement is the length of the total cell track, i.e., the sum of the net displacements between two successive frames ($d_{\text{tot}} = \sum_{i=1}^{N-1} d\left(p_i, p_{i+1}\right)$) (Figure 5.1C) (Table 5.1. Eq. 5.2). Cells can reorient between two frames, such that this measure may underestimate the actual distance traveled. However, we used the same frame rate of 1 min in all experiments, such that the results are comparable with one another. Meandering index is most simply defined as the net distance traveled divided by the total distance traveled (M.I $=\frac{d_{\text{net}}}{d_{\text{tot}}}$) [265] (Figure 5.1C) (Table 5.1. Eq. 5.3). Mean speed is the total displacement divided by traveled time ($\overline{v} = \frac{1}{N-1} \sum_{i=1}^{N-1} v_i$) (Table 5.1. Eq. 5.4). The MSD at time t was calculated for each group by averaging the squared displacement from starting time t_1=1hpw to time t over all cells (K) within that group ($\text{MSD}\,(t) = \frac{1}{K} \sum_{i=1}^{K} d\left(p_{i,1}, p_{i,1+t}\right)^2$) (Figure 5.1D) (Table 5.1. Eq. 5.5). The MSD curve can be used to distinguish migratory behaviours such as Brownian walks and persistent random walks, and analytical expressions for the MSD are known for theoretically ideal random walks. For persistent random walkers, the analytical expression for the MSD is: $MSD\ (t) = 2v^2\ \tau t - 2(v\tau)^2\ (1 - e^{\frac{-t}{\tau}})$) (Table 5.1. Eq. 5.6), with v the intrinsic cell velocity and τ the persistent time, which can be fitted to the MSD calculated from cell tracks [158]. The cell diffusivity constant D and MSD (t) at large t are related through $D = 1/2n\ \frac{dMSD(t)}{\text{dt}}$, with $n = 2$ the dimension, which for persistent random walkers results in $D = 1/2\ v^2\ \tau$ (Table 5.1. Eq. 5.7). Regarding the shape of the MSD curve of our data and the persistent motion reported in leukocyte migration upon tail wounding [266], we assume that distant neutrophils and macrophages behave like persistent random walkers during the time span of imaging. We fit Eq. 5.6 to the MSD curve (Table 5.1. Eq. 5.5) using a non-linear least squares method. The obtained parameters v and τ are then used to compute the approximated cell diffusivity D. For distant neutrophils, the

TABLE 5.1: Formulas of calculated track measures and derived measures

Measure	Definition	
Net displacement (µm)	$d_{\text{net}} = d(p_i, p_N)$	(5.1)
Total displacement (µm)	$d_{\text{tot}} = \sum_{i=1}^{N-1} d(p_i, p_{i+1})$	(5.2)
Meandering index	$M.I. = d_{\text{net}}/d_{\text{tot}}$	(5.3)
Mean speed (µm/min)	$\overline{v} = \frac{1}{N-1} \sum_{i=1}^{N-1} v_i$	(5.4)
Mean squared displacement (µm^2)	$\text{MSD}\ (t) = \frac{1}{K} \sum_{i=1}^{K} (d\ (p_{i,1}\ ,\ p_{i,\ 1+t}))^2$	(5.5)
Fitted mean squared displacement (µm^2)	$\text{MSD}\,(t) = 2v^2\,\tau t - 2\,(v\tau)^2\ \left(1 - e^{\frac{-t}{\tau}}\right)$	(5.6)
Cell diffusivity constant (µm^2/min)	$D = 1/2\ v^2\ \tau$	(5.7)

fit was performed on the first 80 min of tracking, for distant macrophages, the entire 2h tracking period was used.

5.2.6 Statistical analysis

Graphpad Prism software (Version 8.1.1; GraphPad Software, San Diego, CA, USA) was used for statistical analysis. Computations of distance to the wound, MSD and V_{AP} were performed using a Python script including the SciPy stats library for statistical testing. Shaded regions of MSD and V_{AP} over time indicate standard error of mean, the other experiment data are shown as mean ± SD. Statistical significance of differences was determined by using an unpaired, two-tailed t-test for comparing the difference between wild type and *tlr2* and *myd88* mutant. (ns, no significant difference; *P < 0.05; **P < 0.01; ***P < 0.001; ****P < 0.0001).

5.3 Results

5.3.1 Tlr2 and myd88 mutations do not affect development and basal motility of leukocytes.

To determine the leukocyte development in *tlr2* and *myd88* mutants, the double-transgenic line *tlr2*$^{+/+}$ *Tg (mpeg1:mCherry-F);TgBAC (mpx: EGFP)*,

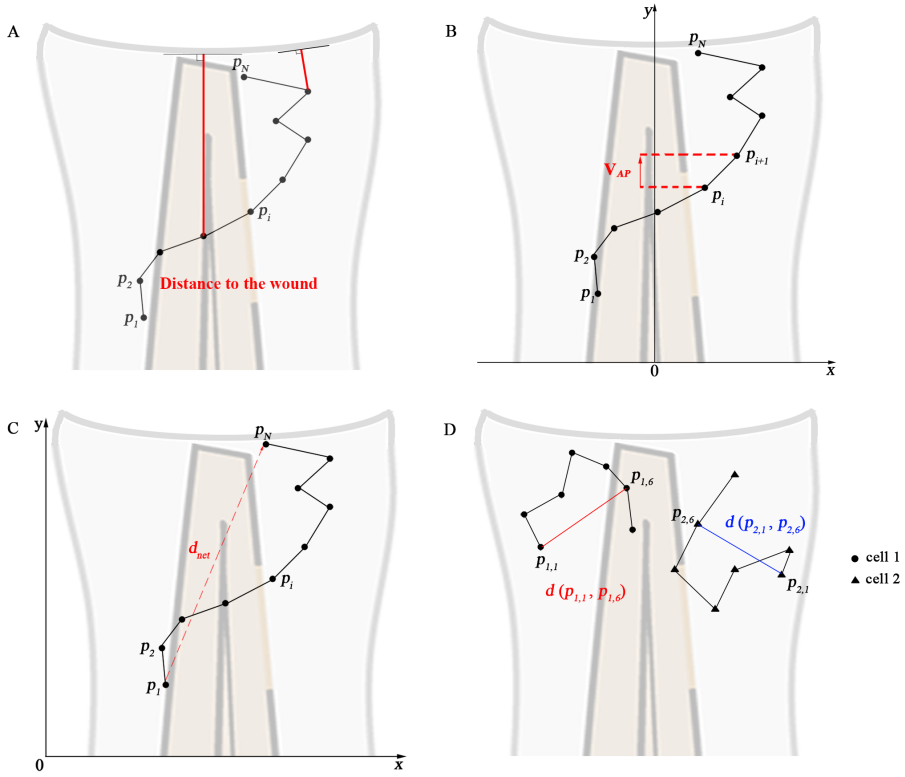

FIGURE 5.1: **Calculated track measures. (A)** Depiction of distance to the wound. It measured for each frame as the shortest distance from the cell's current position to the entire line of the wound, i.e. the orthogonal projection to the wound. **(B)** Depiction of V_{AP}: velocity in anteroposterior axis direction. The visible part of the spine is taken as the y-axis. **(C)** Depiction of the net displacement, total displacement, meandering index and mean speed: the net displacement is the distance of the cell between the first and final time frame. Total displacement is the sum of the net displacement between 2 successive frames. Meandering index corresponds to the net displacement divided by the total displacement and measures the trajectory straightness. Mean speed is the total displacement divided by traveled time. Formulas are shown in Table 5.1. (Eqs. 5.1-5.4). **(D)** Depiction of the construction of the mean squared displacement: the displacement between the first time frame and time frame t from all cells is squared and averaged, see Table 5.1. (Eq. 5.5).

tlr2$^{-/-}$ *Tg (mpeg1:mCherry-F);TgBAC (mpx: EGFP)*, *myd88*$^{+/+}$ *Tg (mpeg1:mCherry-F);TgBAC (mpx: EGFP)* and *myd88*$^{-/-}$ *Tg (mpeg1:mCherry-F);TgBAC (mpx: EGFP)* were constructed. The lines were imaged at 3 dpf to count the number of macrophages and neutrophils in their tail region, and then compared with their wild type siblings (Figure 5.2A). Embryos of the *tlr2* and *myd88* mutants showed similar numbers of macrophages and neutrophils as their wild type siblings (Figures 5.2B- E). This result is consistent with our previous studies of the same *myd88* mutant at 3 dpf and the *tlr2* mutant at 2 dpf [257, 258]. With the aim of investigating the importance of the *tlr2* and the *myd88* mutations for leukocyte behavior under unchallenged condition, the CHT region was analyzed in the double transgenic lines of *tlr2* and *myd88*

FIGURE 5.2 *(following page)*: **Quantification of macrophage and neutrophil numbers and their basal migratory capability in the 3 dpf *tlr2* *and myd88* mutants and wild sibling controls larvae. (A)** Experimental scheme. At 3 dpf, numbers and basal migratory capability of GFP-labeled neutrophils and mCherry-labeled macrophages in tail region were quantified using Leica TCS SP8 confocal laser scanning microscopy (CLSM). Red boxes show the area in which cells were counted or tracked. **(B- E)** The quantification of neutrophil and macrophage numbers in tail region by using *tlr2* and *myd88* zebrafish larvae. Data (mean ± SD) are combined from three pools of zebrafish larvae. No significant differences (ns) in the number of neutrophils (B, D) and macrophages (C, E) was detected with an unpaired, two-tailed t-test. Sample size (n): 28, 32 (B, C); 24, 24 (D, E). **(F- G, J- K)** Quantification of basal migratory capability in 3 dpf *tlr2* zebrafish. The total displacement and mean speed of individual neutrophils (F, J) and macrophages (G, K) were quantified by using a manual tracking plugin. Data (mean ± SD) are combined from three experiments of *tlr2*$^{+/+}$ *Tg (mpeg1:mCherry-F);TgBAC (mpx: EGFP)* and *tlr2*$^{-/-}$ *Tg (mpeg1:mCherry-F);TgBAC (mpx: EGFP)* larvae. No significant differences (ns) in the total displacement and mean speed of neutrophils (F, J) and macrophages (G, K) were detected with an unpaired, two-tailed t-test. Sample size (n): 11, 10 (F, J); 22, 16 (G, K). Cell tracking movies are shown in Supplementary Movie S1-4) **(H- I, L- M)** Quantification of basal migratory capability in 3 dpf *myd88* zebrafish. The total displacement and mean speed of individual neutrophils (H, L) and macrophages (I, M) were quantified by using a manual tracking plugin. Data (mean ± SD) are combined from three experiments of *myd88*$^{+/+}$ *Tg (mpeg1:mCherry-F);TgBAC (mpx: EGFP)* and *myd88*$^{-/-}$ *Tg (mpeg1:mCherry-F);TgBAC (mpx: EGFP)* larvae. No significant differences (ns) in the total displacement and mean speed of neutrophils (H, L) and macrophages (I, M) were detected with an unpaired, two-tailed t-test. Sample size (n): 15, 13 (H, L); 31, 31 (I, M). Cell tracking movies are shown in Supplementary Movie S5-8)

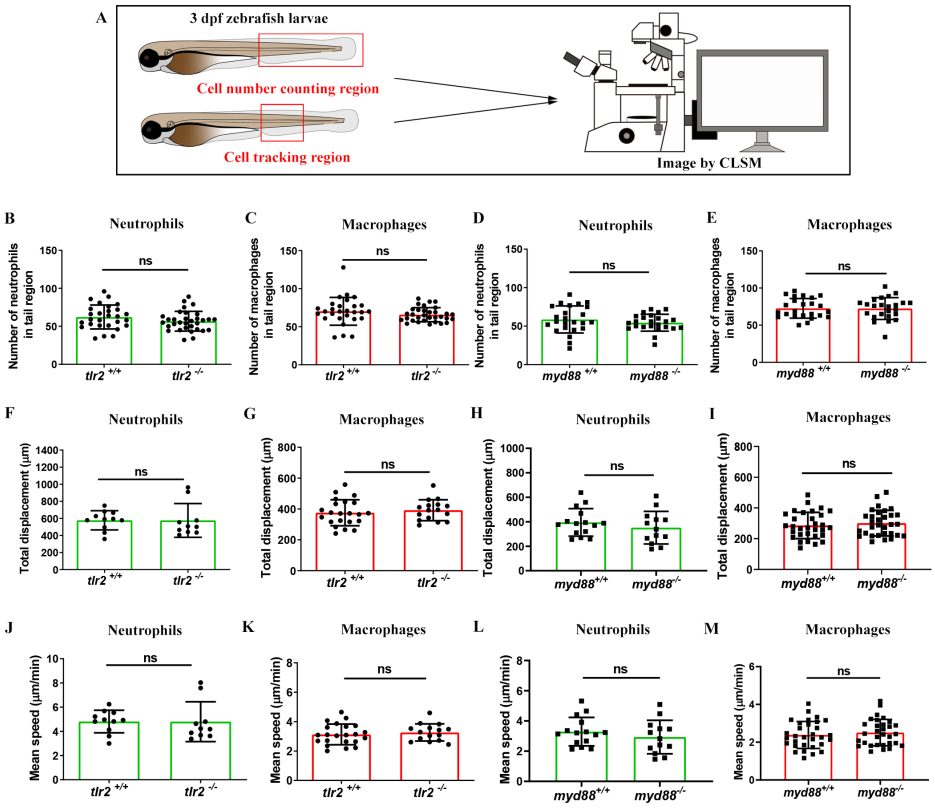
A
3 dpf zebrafish larvae
Cell number counting region
Cell tracking region
Image by CLSM
B
Neutrophils
Number of neutrophils in tail region
ns
tlr2 +/+
tlr2 -/-
C
Macrophages
Number of macrophages in tail region
D
Neutrophils
myd88 +/+
myd88 -/-
E
Macrophages
F
Neutrophils
Total displacement (μm)
G
Macrophages
H
Neutrophils
myd88+/+
myd88-/-
I
Macrophages
J
Neutrophils
Mean speed (μm/min)
K
Macrophages
L
Neutrophils
M
Macrophages

using CLSM by taking time-lapse images (Figure 5.2A). No significant effect was observed on leukocyte basal motility in the CHT tissue in the *tlr2* and *myd88* mutants compared with their wild type sibling control (Figures 5.2F-M). Representative images are shown in Supplementary Figure S5.1 and Supplementary Figure S5.2.

5.3.2 Tlr2 and myd88 regulate neutrophil recruitment to a tail wound

To study the effect of the *tlr2* and *myd88* mutations on the recruitment of neutrophils towards a site of injury, a tail wound method was used in 3 dpf zebrafish larvae as a model for inflammation. To quantify the number of recruited neutrophils to the wound, we counted the number of neutrophils that were located in a range closer than 200 µm from the wound edge of the tail at 1, 2, 4 and 6 hpw (Figure 5.3A). Our results show that the *tlr2* mutation had a significant negative effect on the recruitment of neutrophils after 2, 4 and 6 hpw (Figures 5.3B,C). However, there is no significant difference in recruited neutrophil numbers between wild type and $tlr2^{-/-}$ at 1 hpw (Figures 5.3B,C). Notably, a significant difference of recruited neutrophil numbers was already observed at 1 hpw in *myd88* zebrafish larvae and remained significant until 6 hpw (Figure 5.3D,E).

FIGURE 5.3 *(following page)*: **The number of neutrophils recruited to the wounded area in the *tlr2* and *myd88* mutants and wild type sibling controls larvae. (A)** Experimental scheme. *Tlr2* and *myd88* homozygous mutants and sibling control larvae were wounded at 3 dpf. Their tails were wounded to the tip of the notochord. The red dashed line shows the site of wounding. Recruited neutrophils at the wound were imaged at 1, 2, 4 and 6 hpw by using CLSM. For recruited cell counting analysis, cells localized within an area of 200 µm from the wounding edge toward the body trunk were counted as recruited cells. The red dashed box shows the area where neutrophils were counted as recruited neutrophils. **(B, D)** Representative images of 3 days dpf larvae at 1, 2, 4 and 6 hours post-wounding (hpw). Scale bar: 50 µm. **(C)** Quantification of recruited neutrophil numbers to the wounded area at 1, 2, 4 and 6 hpw in 3dpf $tlr2^{+/+}$ and $tlr2^{-/-}$ larvae. Sample size (n): 45, 46, 82, 72, 74, 68, 50, 50. **(E)** Quantification of recruited neutrophil numbers to the wounded area at 1, 2, 4 and 6 hpw in 3dpf $myd88^{+/+}$ and $myd88^{-/-}$ larvae. Sample size (n): 29, 28, 37, 38, 45, 39, 51, 45. In all cases, statistical analyses were done from 3 independent experiments. An unpaired, two-tailed t-test was used to assess significance (ns, no significant difference, *P < 0.05, **P < 0.01, ***P < 0.001) and data are shown as mean± SD.

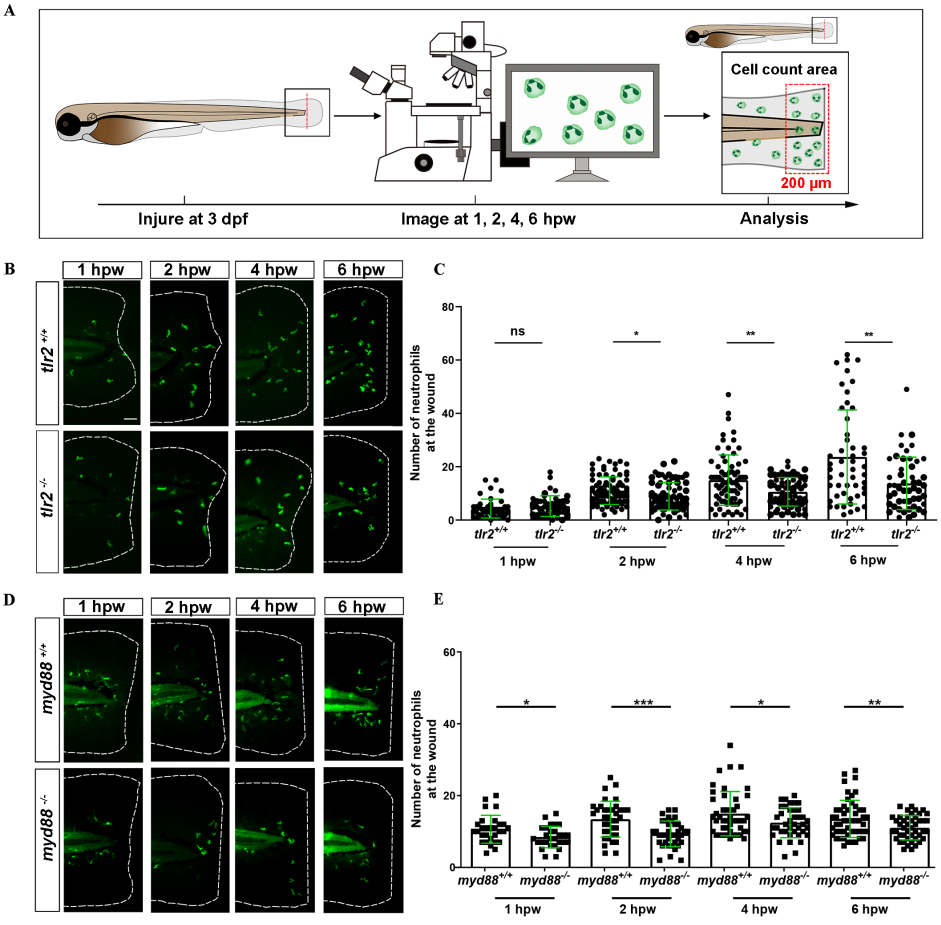
A
Cell count area
200 µm
Injure at 3 dpf
Image at 1, 2, 4, 6 hpw
Analysis
B
1 hpw
2 hpw
4 hpw
6 hpw
tlr2 +/+
tlr2 -/-
C
Number of neutrophils at the wound
ns
*
**
**
tlr2+/+
tlr2-/-
1 hpw
2 hpw
4 hpw
6 hpw
D
myd88 +/+
myd88 -/-
E
*
***
*
**
myd88+/+
myd88-/-

5.3.3 Tlr2 and myd88 regulate macrophage recruitment to a tail wound

To assess the role of the *tlr2* and *myd88* mutations in regulating the recruitment of macrophages to a site of the tail wound, we counted the recruited macrophage numbers by the same method as for measuring the neutrophil recruitment to the wound (Figure 5.4A). Both *tlr2*$^{-/-}$ and *myd88*$^{-/-}$ mutant zebrafish larvae displayed diminished macrophage responses upon wounding (Figure 5.4). Significantly decreased numbers of recruited macrophages toward the injury were measured in the *tlr2*$^{-/-}$ group at 2, 4 and 6 hpw (Figures 5.4B,C). Similarly, there is no significant difference in recruited macrophage numbers between wild type and *tlr2*$^{-/-}$ at 1 hpw (Figure 5.4C). A significant difference of recruited macrophage numbers was already observed from 1 hpw in *myd88* zebrafish larvae, the same as was observed with neutrophil recruitment (Figures 5.4D,E).

5.3.4 Live imaging reveals that the *tlr2* and *myd88* mutations affect distant neutrophil directional persistence, but not migration speed upon tail wounding

To investigate how neutrophils migrate in the absence of *tlr2* or *myd88* after tail wounding, a time-lapse microscopy experiment was performed

FIGURE 5.4 *(following page)*: **The number of macrophages recruited to the wounded area in the *tlr2* and *myd88* mutants and wild type sibling controls larvae. (A)** Experimental scheme. *Tlr2* and *myd88* homozygous mutants and sibling control larvae were wounded at 3 dpf. Their tails were wounded to the tip of the notochord. The red dashed line shows the site of wounding. Recruited macrophages at the wound were imaged at 1, 2, 4 and 6 hpw by using CLSM. For recruited cell counting analysis, cells localized within an area of 200 µm from the wounding edge toward the body trunk were counted as recruited cells. The red dashed box shows the area where macrophages were counted as recruited macrophages. **(B, D)** Representative images of 3 days dpf larvae at 1, 2, 4 and 6 hpw. Scale bar: 50 µm. **(C)** The quantification of recruited macrophage numbers to the wounded area at 1, 2, 4 and 6 hpw in 3dpf *tlr2*$^{+/+}$ and *tlr2*$^{-/-}$ larvae. Sample size (n): 45, 45, 82, 71, 69, 68, 51, 50. **(E)** The quantification of recruited macrophage numbers to the wounded area at 1, 2, 4 and 6 hpw in 3dpf *myd88*$^{+/+}$ and *myd88*$^{-/-}$ larvae. Sample size (n): 35, 34, 40, 43, 56, 42, 60, 58. In all cases, statistical analyses were done with data of 3 independent experiments. An unpaired, two-tailed t-test was used to assess significance (ns, no significant difference, **P < 0.01, ***P < 0.001, ****P < 0.0001) and data are shown as mean± SD.

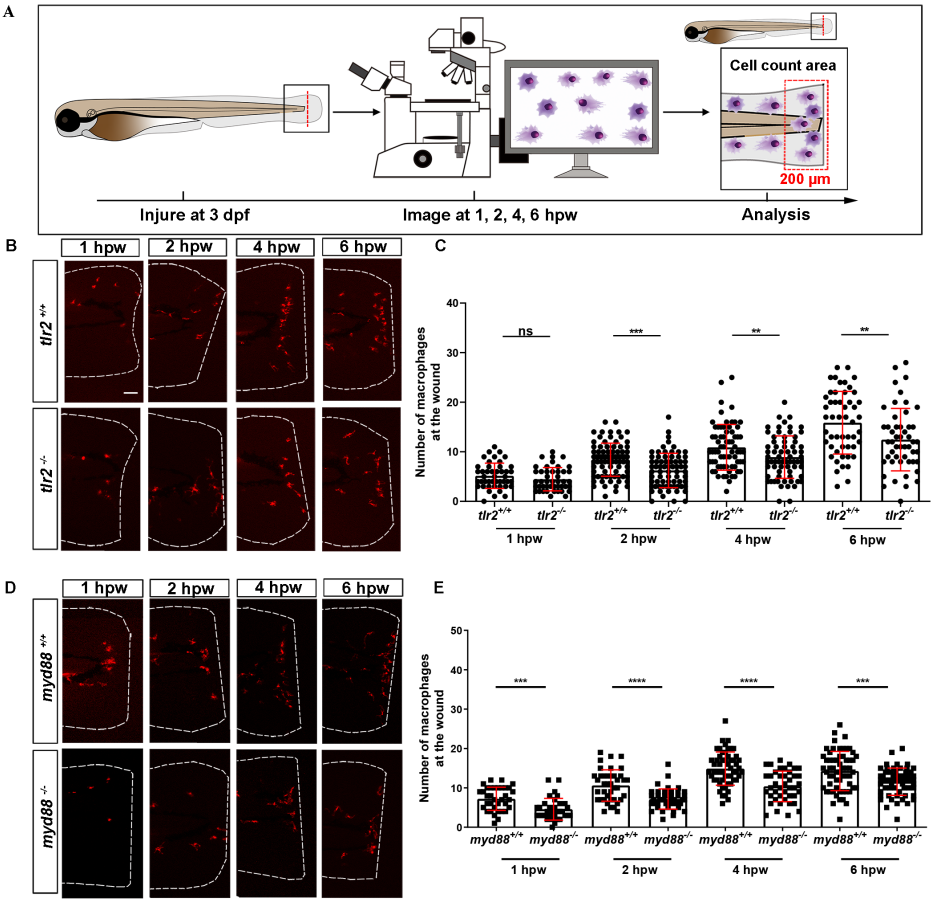
A
Cell count area
200 µm
Injure at 3 dpf
Image at 1, 2, 4, 6 hpw
Analysis
B
1 hpw
2 hpw
4 hpw
6 hpw
tlr2 +/+
tlr2 -/-
C
Number of macrophages at the wound
ns
***
**
**
tlr2+/+
tlr2-/-
1 hpw
2 hpw
4 hpw
6 hpw
D
myd88 +/+
myd88 -/-
E
Number of macrophages at the wound
***
****
****
***
myd88+/+
myd88-/-

by using CLSM between 1 hpw to 3 hpw (Figures 5.5,5.6). The definition of distant and local resident neutrophils was shown in panel A of Figures 5.5,5.6 and Supplementary Figures 5.7,5.8. Neutrophils located closer than 200µm to the wound were defined as local resident neutrophils and further than 200µm were defined as distant neutrophils. Measurement of the distance to the wound over time of all distant neutrophils in the *tlr2*$^{-/-}$ group indicated a trend of impaired infiltration towards the wound (Figures 5.5B,C up panel). In total, the group of distant neutrophils in the *tlr2*$^{+/+}$ group that arrived at the wound edge and stayed within a distance of 20 µm to the wound comprises 84 % of a total of 25 tracked neutrophils (Figure 5.5C up panel). The local resident neutrophils in this group all remained at the wound (Figures 5.7B,C up panel). In contrast, the group of the distant neutrophils in the *tlr2*$^{-/-}$ group that arrived at the wound within 2 h time-lapse cell tracking comprises only approximately 36 % (Figures 5.5B,C bottom panel). Moreover, approximately 33 % of local resident neutrophils in the *tlr2*$^{-/-}$ group already migrated away from the wound edge within 3 hpw (Figures 5.7B,C bottom panel).

FIGURE 5.5 *(following page)*: **Quantification of distant neutrophils behavior in wounded *tlr2* mutant and sibling control larvae. (A)** Experimental scheme. *Tlr2*$^{+/+}$ and *tlr2*$^{-/-}$ larvae were wounded at 3 dpf. The red dashed line shows the site of wounding. Neutrophils of wounded zebrafish larvae were tracked for 2 h and images were taken every 1 min by using CLSM. For cell tracking analysis, cells localized outside an area of 200 µm from the wounding edge toward the body trunk were counted as distant cells. Blue dashed box shows the area where distant neutrophils were tracked. **(B)** Representative images of distant neutrophil tracks in the wounded tail fin of 3 dpf *tlr2*$^{+/+}$ or *tlr2*$^{-/-}$ larvae at frame 1, frame 60 and frame 120. Time interval between two successive frames is 1 min. Each color track represents an individual neutrophil. Cell tracking movies are shown in Supplementary Movie S9-10). Scale bar: 50 µm. **(C)** Distance to the wound. Black dash line represents average distance to the wound. Each color line represents one cell. **(D-I)** Quantification of distant neutrophil tracks. There was no significant difference between the groups in terms of mean speed (D), net displacement (E) and MSD (green) and fitted MSD (black) (G). However, meandering index (F) and mean V_{AP} (H) of neutrophils at the wound in *tlr2*$^{+/+}$ is greater than in *tlr2*$^{-/-}$ larvae. The fitted MSD (G, black) was fitted for $dt < 80$ min. The shaded regions in MSD (G) and mean V_{AP} over time (I) indicate standard error of the mean. Statistical analyses were done with 7 and 8 fish respectively for each group. An unpaired, two-tailed t-test was used to assess significance (ns, non-significance, *P < 0.05) and data are shown as mean± SD. Sample size (n): 25, 22 (D, E, F, H).

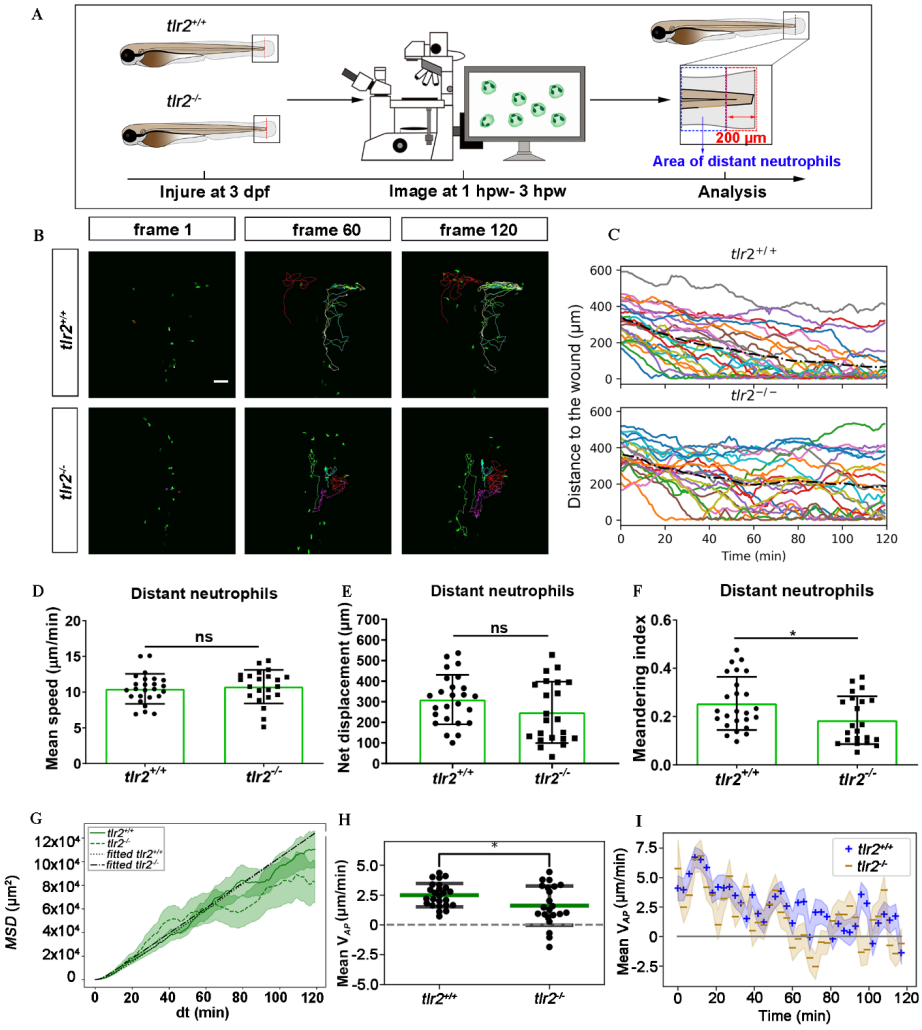
A
tlr2+/+
tlr2-/-
200 µm
Area of distant neutrophils
Injure at 3 dpf
Image at 1 hpw- 3 hpw
Analysis
B
frame 1
frame 60
frame 120
C
Distance to the wound (µm)
Time (min)
D
Distant neutrophils
Mean speed (µm/min)
ns
E
Distant neutrophils
Net displacement (µm)
ns
F
Distant neutrophils
Meandering index
*
G
MSD (µm²)
dt (min)
H
Mean VAP (µm/min)
*
I
Mean VAP (µm/min)
Time (min)

In general, distant neutrophils in the *myd88*$^{+/+}$ group showed more chemotaxis to the wound compared to *myd88*$^{-/-}$ neutrophils (Figures 5.6B,C). Approximately 96% distant neutrophils arrived at the wound (within a distance of 20 µm to the wound) in the *myd88*$^{+/+}$ group in total (Figure 5.6C up panel). However, only 70% distant neutrophils arrived to the wound (within a distance of 20 µm to the wound) in the *myd88*$^{-/-}$ group. (Figure 5.6C bottom panel). The local resident neutrophils in this group all remained at the wound except for a few outliers (Figures 5.8C). In summary, the general trend of distant neutrophils migration in the *myd88* mutant and sibling zebrafish groups was consistent with the result in the *tlr2* mutant and sibling zebrafish groups, respectively (Figure 5.6C).

To quantify differences in neutrophil migration behavior between *tlr2* and *myd88* mutants and their wild type siblings, we first analyzed whether the deficiency of *tlr2* and *myd88* can affect neutrophil mean migration speed upon wounding. The results showed that the *tlr2* and the *myd88* mutations do not affect the mean speed of both distant and local resident neutrophils

FIGURE 5.6 *(following page)*: **Quantification of distant neutrophils behavior in wounded *myd88* mutant and sibling control larvae. (A)** Experimental scheme. *Myd88*$^{+/+}$ and *myd88*$^{-/-}$ larvae were wounded at 3 dpf. The red dashed line shows the site of wounding. Neutrophils of wounded *myd88* zebrafish larvae were tracked for 2 h and images were taken every 1 min by using CLSM. For cell tracking analysis, cells localized outside an area of 200 µm from the wounding edge toward the body trunk were counted as distant cells. Blue dashed box shows the area where distant neutrophils were tracked. **(B)** Representative images of distant neutrophil tracks in the wounded tail fin of 3 dpf *myd88*$^{+/+}$ or *myd88*$^{-/-}$ larvae at frame 1, frame 60 and frame 120. Time interval between two successive frames is 1 min. Each color track represents an individual neutrophil. Cell tracking movies are shown in Supplementary Movie S11-12). Scale bar: 50 µm. **(C)** Distance to the wound. Black dash line represents average distance to the wound. Each color line represents one cell. **(D-I)** Quantification of distant neutrophil tracks. There was no significant difference between the groups in terms of mean speed (D). However, the net displacement (E), meandering index (F),), MSD (green) and fitted MSD (black) (G) and mean V_{AP} (H) of neutrophils at the wound in *myd88*$^{+/+}$ is greater than in *myd88*$^{-/-}$ larvae. The shaded regions MSD (G) and in mean V_{AP} over time (I) indicate standard error of the mean. The fitted MSD (G, black) was fitted for $dt < 80$ min. Statistical analyses were done with 6 and 4 fish respectively for each group. An unpaired, two-tailed t-test was used to assess significance (ns, non-significance, **P < 0.01) and data are shown as mean± SD. Sample size (n): 23, 10 (D, E, F, H).

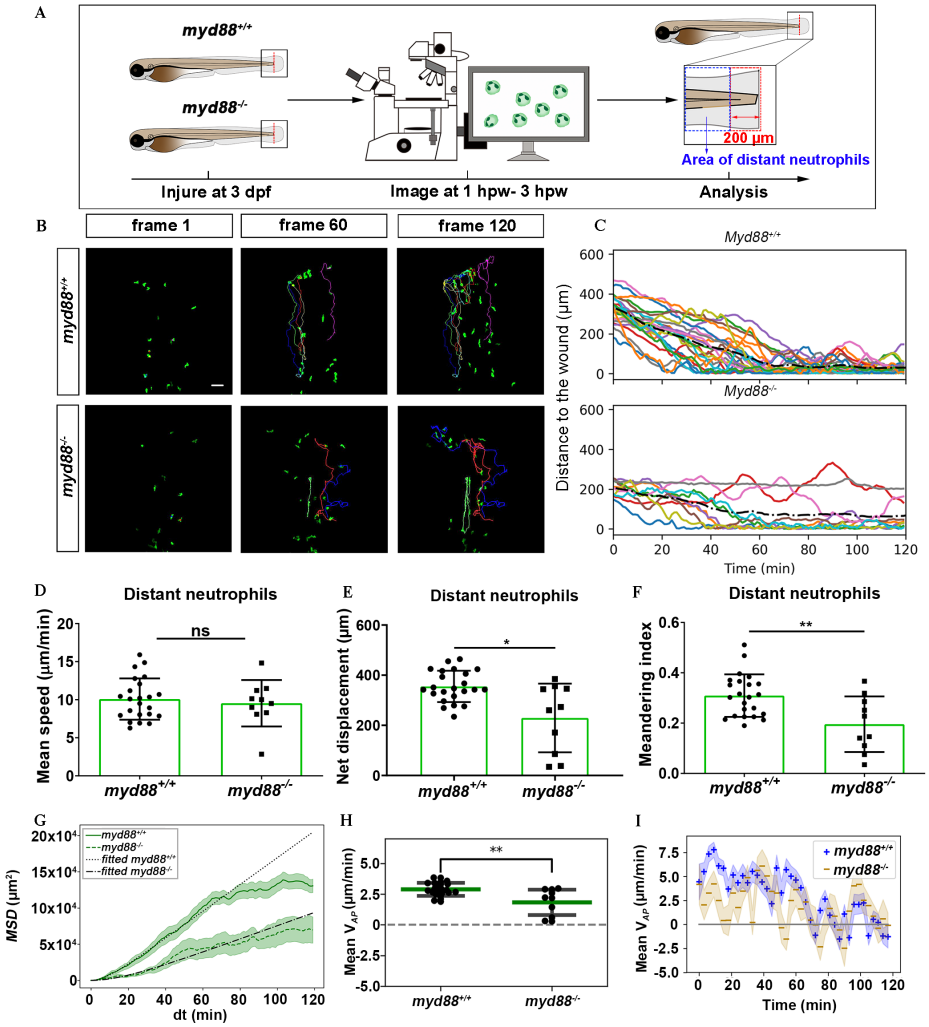
A
myd88+/+
myd88-/-
200 µm
Area of distant neutrophils
Injure at 3 dpf
Image at 1 hpw- 3 hpw
Analysis
B
frame 1
frame 60
frame 120
myd88+/+
myd88-/-
C
Myd88+/+
Myd88-/-
Distance to the wound (µm)
Time (min)
D
Distant neutrophils
Mean speed (µm/min)
ns
myd88+/+
myd88-/-
E
Distant neutrophils
Net displacement (µm)
*
F
Distant neutrophils
Meandering index
**
G
MSD (µm²)
myd88+/+
myd88-/-
fitted myd88+/+
fitted myd88-/-
dt (min)
H
Mean VAP (µm/min)
**
I
Mean VAP (µm/min)
myd88+/+
myd88-/-
Time (min)

TABLE 5.2: Persistence time, intrinsic cell velocity and diffusivity obtained by fitting Eq. 5.6 to the MSD curves.

Neutrophils	τ (min)	v (μm/min)	D (μm^2/min)	Fitted time-frame
tlr2$^{+/+}$	6.88 ± 0.23	8.98 ± 0.12	277	$t \leq 80$
tlr2$^{-/-}$	3.24 ± 0.35	12.80 ± 0.59	265	
myd88$^{+/+}$	6.83 ± 0.34	10.97 ± 0.22	410	
myd88$^{-/-}$	5.04 ± 0.49	10.33 ± 0.42	269	

upon the wounding (Figure 5.5D; Figures 5.6D; Supplementary Figures 5.7D and Supplementary Figures 5.8D).

We also tested the effect of the *tlr2* and the *myd88* mutations on the movement direction of neutrophils upon wounding by the quantification of net displacement, whose definition is shown in Figure 5.1 and Table 5.1. We observed that the net displacement of distant neutrophils had a decreased trend in the *tlr2*$^{-/-}$ group compared to the *tlr2*$^{+/+}$ group (Figure 5.5E). Moreover, cell diffusivity D determined by fitting Eq. 5.6 to the MSD curve (Table 5.1) did not differ much between the *tlr2*$^{-/-}$ group and the *tlr2*$^{+/+}$ group (Figure 5.5G, Table 5.2). A significant decrease in net displacements was consistently observed in the *myd88* mutant group (Figure 5.6E). Also, *myd88*$^{-/-}$ neutrophils have lower diffusivity than *myd88*$^{+/+}$ neutrophils as measured from fitting Eq. 5.6 to the MSD plots (Figure 5.6G, Table 5.2). As the cell speed of *myd88*$^{-/-}$ neutrophils does not differ from that of *myd88*$^{+/+}$ neutrophils (Figure 5.6D), the reduced diffusivity may be due to more frequent or sharper changes of direction of the *myd88*$^{-/-}$ neutrophils. Preliminary results in analysing the angles between consecutive time frames suggest that the *myd88*$^{-/-}$ neutrophils indeed have sharper turns than their wild type siblings. As neutrophils reach the wound edge, their diffusivity is limited in space. With the initial distance of the distant neutrophils in min, the maximum of MSD(t) is expected around $12 \times 10^4 \mu m^2/min$, which is also visible in the flattening of the MSD at later time frames. We therefore limited fitting Eq. 5.6 to the MSD curve to $dt < 80$.

To further study the effect of the *tlr2* and *myd88* mutations on the neutrophil migration direction, we determined the meandering index and mean V_{AP} (Figures 5.5F,H and Figures 5.6F,H). The meandering index and mean V_{AP} are all significantly decreased in the distant neutrophils of both *tlr2*$^{-/-}$ and *myd88*$^{-/-}$ mutants compared to their wild type sibling controls (Figures 5.5F,H and Figures 5.6F,H). However, no significant difference of meandering index was found in local resident neutrophils of the *tlr2*$^{-/-}$

and *myd88*$^{-/-}$ mutants compared to the wild type siblings (Figures 5.7F and 5.8F). The mean V_{AP} over time qualitatively shows again the impaired chemotaxis of *tlr2*$^{-/-}$ and *myd88*$^{-/-}$ neutrophils compared to the *tlr2*$^{+/+}$ and *myd88*$^{+/+}$ neutrophils, respectively (Figure 5.5I and Figure 5.6I). As more and more neutrophils approach the wound (Figure 5.5C,5.6), the mean V_{AP} drops. For almost every time point, mean V_{AP} of *tlr2*$^{+/+}$ exceeds mean V_{AP} of *tlr2*$^{-/-}$(Figure 5.5I). Similar results were observed for *myd88*$^{+/+}$ and *myd88*$^{-/-}$ distant neutrophils (Figure 5.6I).

5.3.5 Live imaging reveals that the *tlr2* and *myd88* mutations affect distant macrophage migration speed and directional persistence upon tail wounding

To study the effect of the *tlr2* and *myd88* mutations on macrophage migration upon wounding, we compared macrophage behavior with their wild type siblings. The definition of distant macrophage and local resident macrophage was shown in panel A of Figures 5.9 , 5.10, 5.11, and 5.12. Macrophages located closer than 200µm to the wound were defined as local resident macrophages and further than 200µm were defined as distant macrophages. In contrast to neutrophils, the majority of macrophages do not reach the wound within the measured time period. By measuring their distance to the wound over time, we can see a trend that distant macrophages show less chemotaxis in the *tlr2*$^{-/-}$ and *myd88*$^{-/-}$ mutant groups compared to their wild type sibling groups (Figures 5.9B,C and Figures 5.10B,C). Within 50 µm to the wound, the local resident macrophages all remained at the wound in both the *tlr2* and *myd88* mutants and their wild type sibling controls (Figures 5.11B,C and Figures 5.12B,C). Within a distance of 200 µm, but outside 50 µm to the wound, local resident macrophages tend to migrate to the wound direction (Figures 5.11B,C and Figures 5.12B,C).

To quantify differences in macrophage migration behavior between *tlr2* and *myd88* mutants and their wild type siblings, we first analyzed whether the deficiency of *tlr2* and *myd88* can affect macrophage mean migration speed upon wounding. Following tail wounding, both distant and local resident macrophages migrate more slowly in the *tlr2*$^{-/-}$ and *myd88*$^{-/-}$ mutant groups than in the wild type sibling controls (Figure 5.9D; Figure 5.10D; Figure 5.11D; Figure 5.12D).

Subsequently, we studied the directional persistence of macrophage migration upon wounding. To this end, we quantified the net displacement, meandering index and mean V_{AP} in the *tlr2* and *myd88* mutants and siblings. The net displacement of the distant macrophages (Table 5.1. Eq. 5.1) was reduced in the *tlr2*$^{-/-}$ and *myd88*$^{-/-}$ mutants compared to the controls

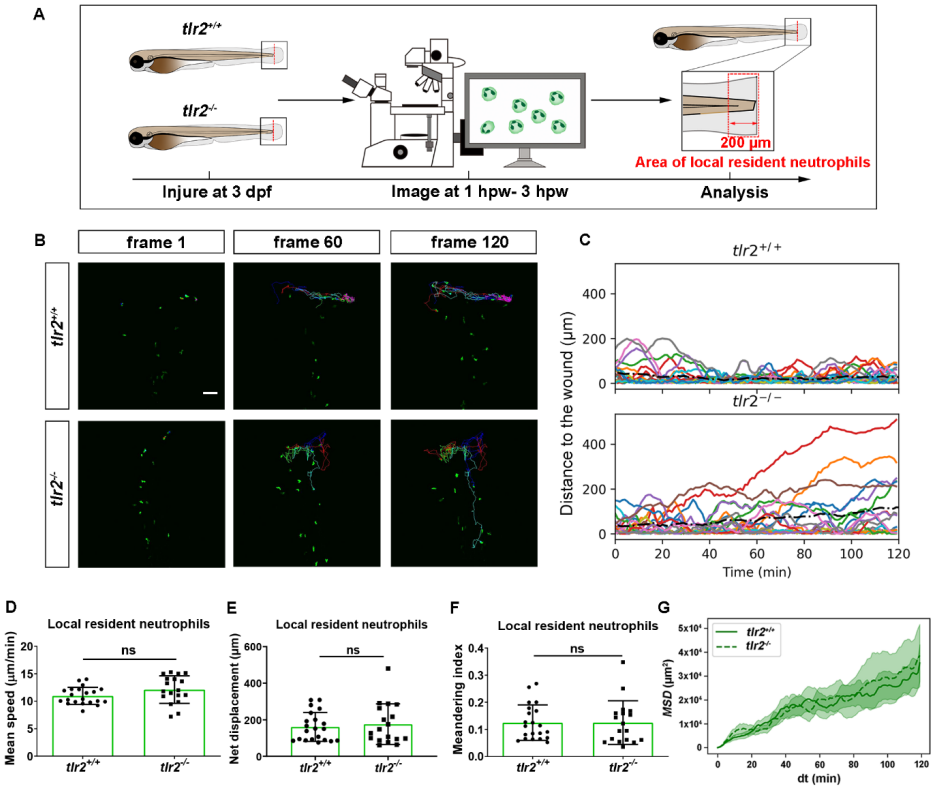

FIGURE 5.7: **Quantification of localized resident neutrophils behavior in wounded *tlr2* larvae. (A)** Experimental scheme. **(B)** Representative images of local resident neutrophils tracks in the wounded tail fin of 3 dpf *tlr2*$^{+/+}$ or *tlr2*$^{-/-}$ larvae at frame 1, frame 60 and frame 120. Cell tracking movies are shown in Supplementary Movie S17-18). Scale bar: 50 µm. **(C)** Distance to the wound. Black dash line represents average distance to the wound. Each color line represents one cell. **(D-I)** Quantification of local resident neutrophil tracks, mean speed (D); net displacement (E); Meandering index (F); MSD (G). An unpaired, two-tailed t-test was used to assess significance (ns, non-significance) and data are shown as mean± SD.

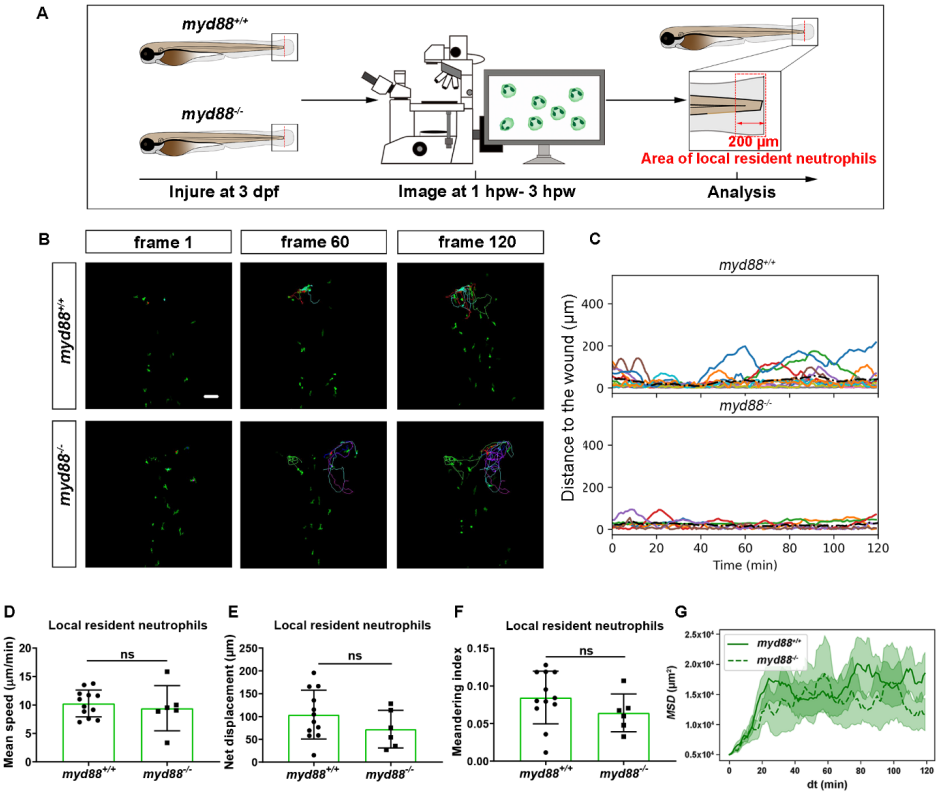

FIGURE 5.8: **Quantification of localized resident neutrophils behavior in wounded *myd88* larvae. (A)** Experimental scheme. **(B)** Representative images of local resident neutrophils tracks in the wounded tail fin of 3 dpf *myd88*$^{+/+}$ or *myd88*$^{-/-}$ larvae at frame 1, frame 60 and frame 120. Cell tracking movies are shown in Supplementary Movie S19-20). Scale bar: 50 µm. **(C)** Distance to the wound. Black dash line represents average distance to the wound. Each color line represents one cell. **(D-I)** Quantification of local resident neutrophil tracks, mean speed (D); net displacement (E); Meandering index (F); MSD (G). An unpaired, two-tailed t-test was used to assess significance (ns, non-significance) and data are shown as mean± SD.

(Figure 5.9E; Figure 5.10E). Furthermore, the meandering index (Table 5.1. Eq. 5.3) was also significantly decreased in the *tlr2*$^{-/-}$ and *myd88*$^{-/-}$ groups (Figures 5.9F,H and Figures 5.10), indicating that the decrease in net displacement was not only due to a reduced speed, but also due to loss of directionality. This is also supported by the significantly reduction in mean V_{AP} of distant macrophages in the *tlr2*$^{-/-}$ and *myd88*$^{-/-}$ groups (Figures 5.9F,H and Figures 5.10). However, no significant differences in net displacement were found in local resident *tlr2* and *myd88* macrophage groups (Supplementary Figure 5.11E and Supplementary Figure 5.12E). The trend of mean V_{AP} over time is similar to the one observed for distant neutrophils, in that *tlr2*$^{+/+}$ and *myd88*$^{+/+}$ macrophages have a higher mean V_{AP} than *tlr2*$^{-/-}$ and *myd88*$^{-/-}$ macrophages during the entire tracking period. The mean V_{AP} of macrophages is positive for a longer period of time compared to the neutrophils, as the majority of macrophages have not reached the wound site during the 2h time span.

The differences in speed and directionality also became apparent from the differences in MSD between the *tlr2*$^{+/+}$ and *myd88*$^{+/+}$ distant macrophages versus the *tlr2*$^{-/-}$ and *myd88*$^{-/-}$ distant macrophages (Figures 5.9G,5.10G).

FIGURE 5.9 *(following page)*: **Quantification of distant macrophage behavior in wounded *tlr2* mutant and sibling control larvae. (A)** Experimental scheme. *Tlr2*$^{+/+}$ and *tlr2*$^{-/-}$ larvae were wounded at 3 dpf. The red dashed line shows the site of wounding. Macrophages of wounded *tlr2* zebrafish larvae were tracked for 2 h and images were taken every 1 min by using CLSM. For cell tracking analysis, cells localized outside an area of 200 µm from the wounding edge toward the body trunk were counted as distant cells. Blue dashed box shows the area where distant macrophages were tracked. **(B)** Representative images of distant macrophage tracks in the wounded tail fin of 3 dpf *tlr2*$^{+/+}$ or *tlr2*$^{-/-}$ larvae at frame 1, frame 60 and frame 120. Time interval between two successive frames is 1 min. Each color track represents an individual macrophage. Cell tracking movies are shown in Supplementary Movie S13-14). Scale bar: 50 µm. **(C)** Distance to the wound. Black dash line represents average distance to the wound. Each color line represents one cell. **(D-I)** Quantification of distant macrophage tracks. There was a significant difference between the groups in terms of mean speed (D), net displacement (E), meandering index (F),), MSD (red) and fitted MSD (black) (G) and mean V_{AP} (H) of macrophages. The shaded regions in MSD (G) and mean V_{AP} over time (I) indicate standard error of the mean. Statistical analyses were done with 6 and 8 fish respectively for each group. An unpaired, two-tailed t-test was used to assess significance (ns, non-significance, *P < 0.05, **P < 0.01, ****P < 0.0001) and data are shown as mean± SD. Sample size (n): 23, 22 (D, E, F, H).

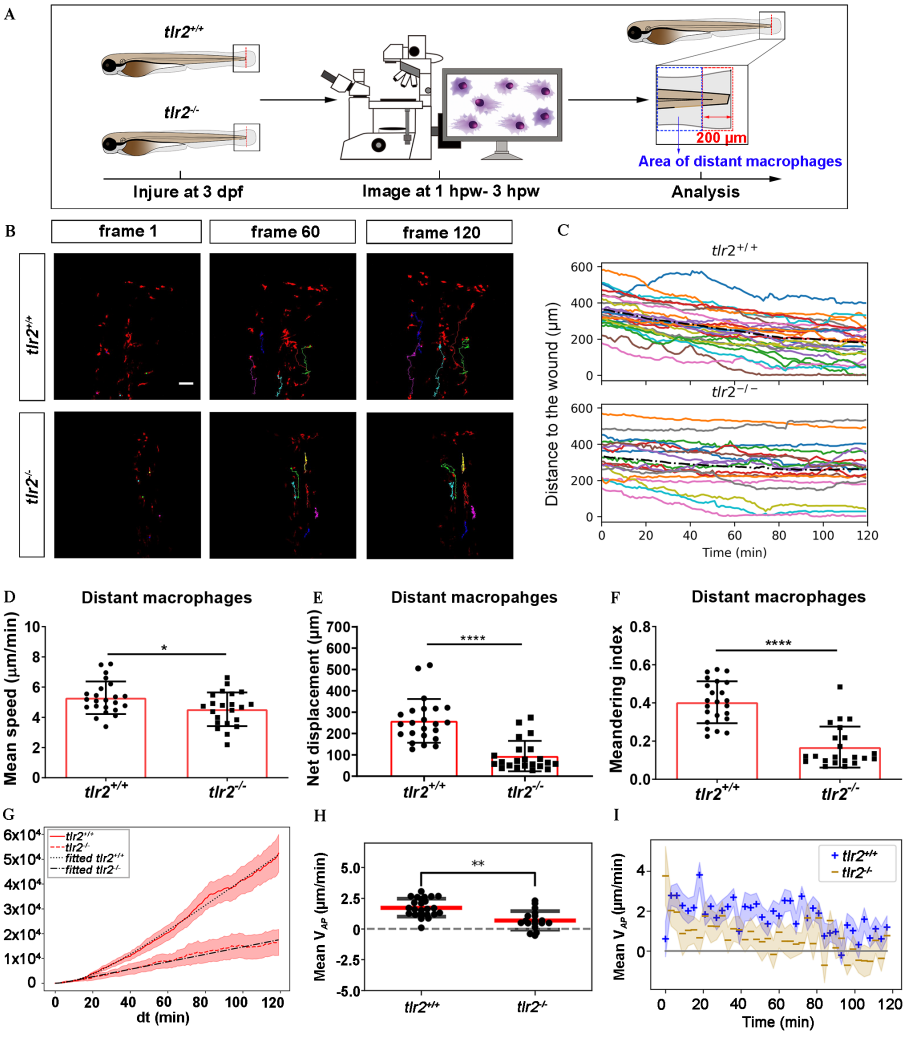
A
tlr2+/+
tlr2-/-
200 µm
Area of distant macrophages
Injure at 3 dpf
Image at 1 hpw- 3 hpw
Analysis
B
frame 1
frame 60
frame 120
C
Distance to the wound (µm)
Time (min)
D
Distant macrophages
Mean speed (µm/min)
E
Distant macropahges
Net displacement (µm)
F
Distant macrophages
Meandering index
G
MSD (µm²)
dt (min)
H
Mean VAP (µm/min)
I
Mean VAP (µm/min)
Time (min)

The MSD (Table 5.1. Eq. 5.5) is lower for the *tlr2*$^{-/-}$ and *myd88*$^{-/-}$ macrophages, which can reflect a speed reduction and/or a lowered directional persistence. A decreased directional persistence can also be seen through the shape of the MSD curve. For *tlr2*$^{+/+}$ and *myd88*$^{+/+}$ distant macrophages, the MSD curve, especially at short time intervals dt, has a parabolic shape, indicating straight cell trajectories. For *tlr2*$^{-/-}$, however, the MSD curve has a more linear shape, indicating random and non-persistent cell motility. The persistence time obtained from fitting Eq. 5.6, confirms this observation with an order of magnitude lower persistence time for the *tlr2*$^{-/-}$ macrophages compared to their wild type siblings group (Table 5.3). For the *myd88* groups, the persistence time is of the same order but larger in *myd88*$^{-/-}$ macrophages, which in turn have a lower intrinsic cell velocity v (Table 5.3). Consequently, the cell diffusivity D is also decreased in the *tlr2*$^{-/-}$ and *myd88*$^{-/-}$ macrophage groups compared to the *tlr2*$^{+/+}$ and *myd88*$^{+/+}$ macrophage groups. In summary, the data show that both *tlr2* and *myd88* mutations affect distant macrophage migration speed and directional persistence upon tail wounding.

FIGURE 5.10 *(following page)*: **Quantification of distant macrophages behavior in wounded *myd88* mutant and sibling control larvae. (A)** Experimental scheme. *Myd88*$^{+/+}$ and *myd88*$^{-/-}$ larvae were wounded at 3 dpf. The red dashed line shows the site of wounding. Macrophages of wounded zebrafish larvae were tracked for 2 h and images were taken every 1 min by using CLSM. For cell tracking analysis, cells localized outside an area of 200 µm from the wounding edge toward the body trunk were counted as distant cells. Blue dashed box shows the area where distant macrophages were tracked. **(B)** Representative images of distant macrophage tracks in the wounded tail fin of 3 dpf *myd88*$^{+/+}$ or *myd88*$^{-/-}$ larvae at frame 1, frame 60 and frame 120. Time interval between two successive frames is 1 min. Each color track represents an individual macrophage. Cell tracking movies are shown in Supplementary Movie S15-16). Scale bar: 50 µm. **(C)** Distance to the wound. Black dash line represents average distance to the wound. Each color line represents one cell. **(D-I)** Quantification of distant macrophage tracks. There was a significant difference between the groups in terms of mean speed (D), net displacement (E), meandering index (F), MSD (red) and fitted MSD (black) (G) and mean V_{AP} (H) of macrophages. Statistical analyses were done with 6 and 5 fish respectively for each group. The shaded regions in MSD (G) and mean V_{AP} over time (I) indicate standard error of the mean. An unpaired, two-tailed t-test was used to assess significance (ns, non-significance, *P < 0.05, **P < 0.01, ****P < 0.0001) and data are shown as mean± SD. Sample size (n): 32, 26 (D, E, F, H).

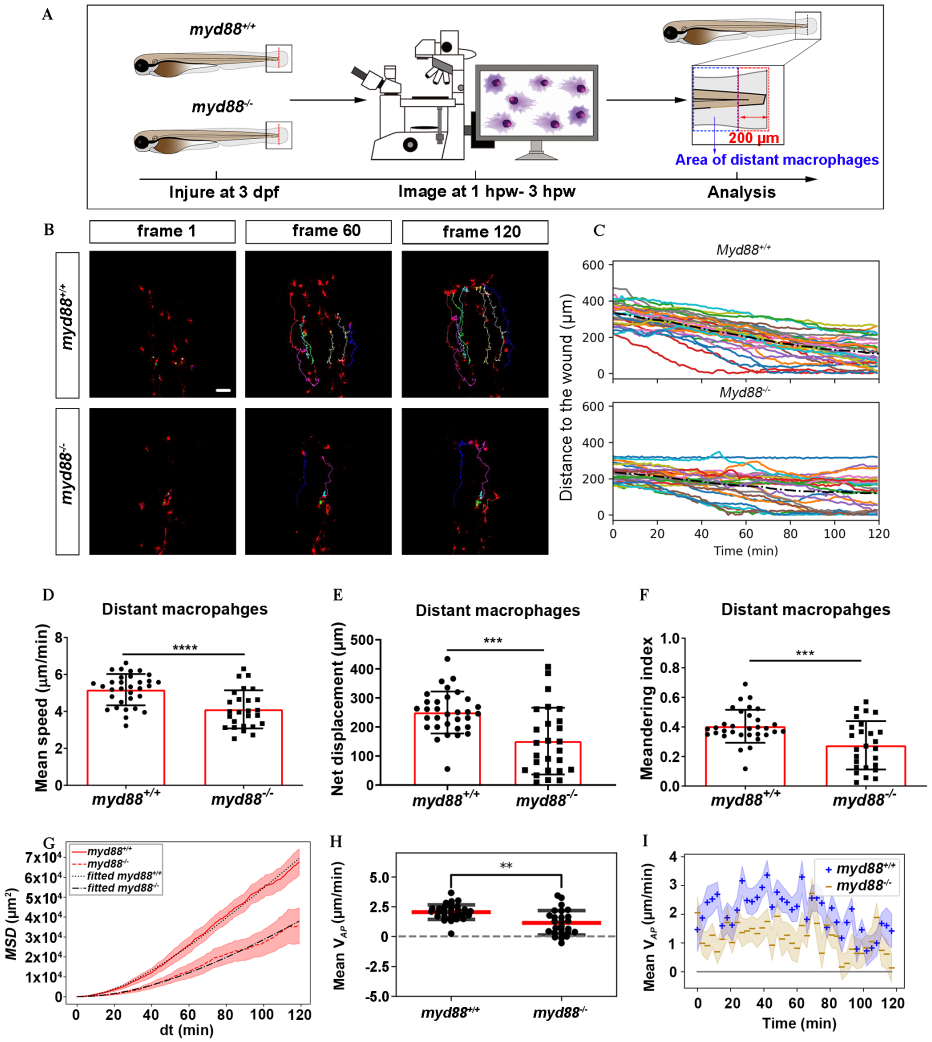

TABLE 5.3: Persistence time, intrinsic cell velocity and diffusivity obtained by fitting Eq. 5.6 to the MSD curves of distance macrophages.

Macrophages	τ (min)	v (µm/min)	D (µm^2/min)	Fitted time-frame
tlr2$^{+/+}$	20.83 ± 0.87	3.56 ± 0.04	132	$t \leq 120$
tlr2$^{-/-}$	2.47 ± 0.23	5.51 ± 0.23	38	
myd88$^{+/+}$	61.38 ± 3.81	3.04 ± 0.03	284	
myd88$^{-/-}$	104.36 ± 14.35	2.06 ± 0.03	221	

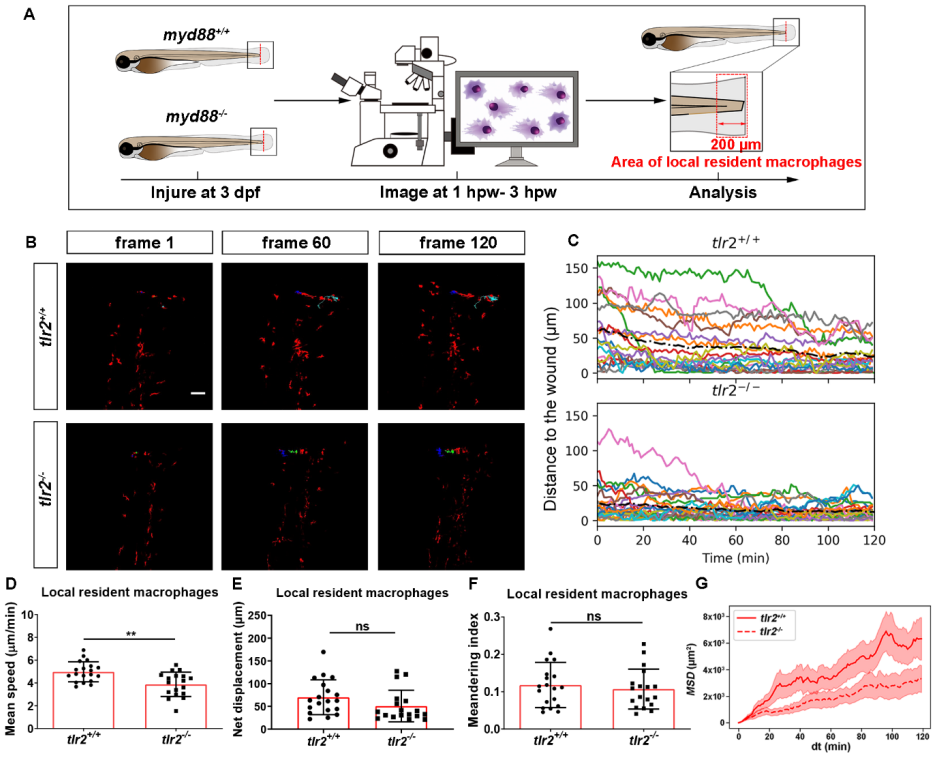

FIGURE 5.11: **Quantification of localized resident macrophages behavior in wounded *tlr2* larvae. (A)** Experimental scheme. **(B)** Representative images of local resident macrophages tracks in the wounded tail fin of 3 dpf *tlr2*$^{+/+}$ or *tlr2*$^{-/-}$ larvae at frame 1, frame 60 and frame 120. Cell tracking movies are shown in Supplementary Movie S21-22). Scale bar: 50 µm. **(C)** Distance to the wound. Black dash line represents average distance to the wound. Each color line represents one cell. **(D-I)** Quantification of local resident macrophage tracks, mean speed (D); net displacement (E); Meandering index (F); MSD (G). An unpaired, two-tailed t-test was used to assess significance (ns, non-significance) and data are shown as mean± SD.

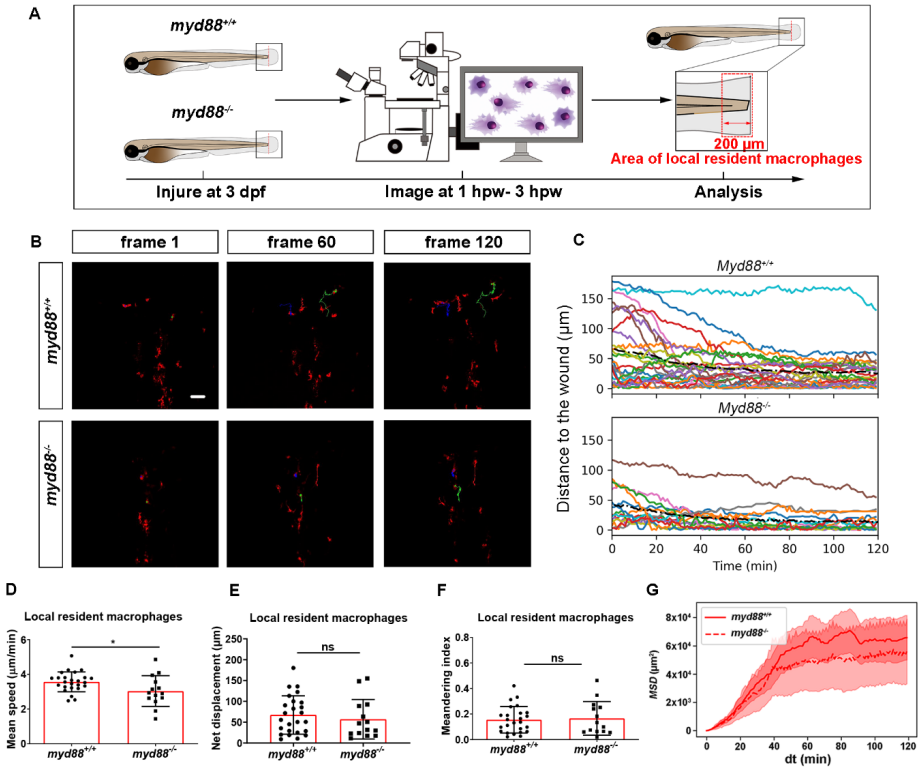

FIGURE 5.12: **Quantification of localized resident macrophages behavior in wounded *myd88* larvae. (A)** Experimental scheme. **(B)** Representative images of local resident macrophages tracks in the wounded tail fin of 3 dpf *myd88*$^{+/+}$ or *myd88*$^{-/-}$ larvae at frame 1, frame 60 and frame 120. Scale bar: 50 µm. **(C)** Distance to the wound. Black dash line represents average distance to the wound. Each color line represents one cell. Cell tracking movies are shown in Supplementary Movie S23-24). **(D-I)** Quantification of local resident macrophage tracks, mean speed (D); net displacement (E); Meandering index (F); MSD (G). An unpaired, two-tailed t-test was used to assess significance (ns, non-significance) and data are shown as mean± SD.

5.4 Discussion

In this study we visualized cell migration in *tlr2* and *myd88* mutants using live-imaging in a zebrafish tail wounding model. Thereby we demonstrated that these genes play a crucial role to control the migration of both neutrophils and macrophages upon tissue wounding. Like in mammals, neutrophils and macrophages play a dominant role in the wounding response during the first several hours after zebrafish tail fin wounding [267, 215, 252]. In mice, it has been shown previously that TLR signaling plays a role in controlling infiltration of neutrophils and macrophages into injured tissue [233, 234, 235, 236]. The function of TLR signaling in migration to epithelial wounds has only been studied so far in zebrafish larvae [242]. This study found that knock-down of *myd88* by morpholinos impairs the infiltration of neutrophils into the wound area, but the mechanisms underlying such reduced wound infiltration remained unknown. By using double transgenic lines, here we show that *tlr2* and *myd88* are both essential for directed migration of distant neutrophils and macrophages to the wounded tissue. The meandering index (Figure 5.1 and Table 5.1. Eq. 5.3) of distant neutrophils and macrophages was significantly decreased in *tlr2* and *myd88* mutant larvae compared with wild type sibling control groups (Figures 5.5F, 5.6F, 5.9F and 5.10F). Moreover, the migration speed of distant and local resident macrophages was decreased upon wounding in the *tlr2* and *myd88* mutants (Figures 5.9D and 5.10D; Supplementary Figures 5.115D and 5.126D), but not in unchallenged larvae. Taken together, these data suggest that TLR signaling is implicated in the sensitivity to signaling molecules secreted by the wound, explaining why less infiltration of neutrophils and macrophages is observed in tail wounds of the *tlr2* and *myd88* mutants (Figure 5.13).

The difference in directional persistence of the distant neutrophils and macrophages in the mutant shows already within 3 hours post wounding, suggesting that TLR signaling is involved in direct sensing of signals from the wound at the post-transcriptional level. However, since TLRs have not been implied in sensing meandering gradients, we assume that this function involves other receptors. Tlr2 has been shown to be essential for the regulation of cytokines and chemokines expression in both mice and zebrafish [236, 258]. For instance, we have shown that *tlr2* mutant shows a significant lower expression of *cxcl11aa* and also of a related chemokine, *cxcl11ac*, during mycobacterial infection. The CXCR3-CXCL11 chemokine-signaling axis has been demonstrated to play an essential role not only in infection process and but also in inflammation process by regulating leukocyte trafficking [264, 255]. It is possible that an insufficient level of

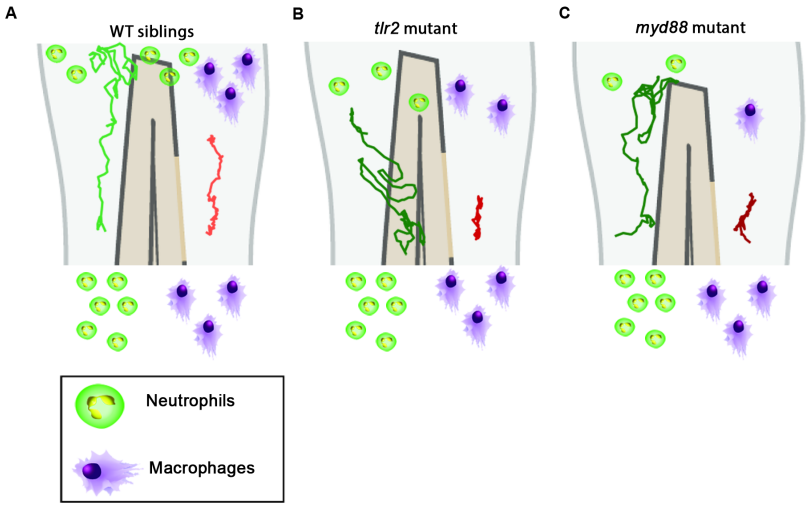

FIGURE 5.13: **Graphic summary of the data of cell migration behavior in the *tlr2* and *myd88* mutants and wild type siblings. (A)** Cell migration behavior in the wild type siblings. **(B)** Cell migration behavior in the *tlr2* mutant. **(C)** Cell migration behavior in the *myd88* mutant. In all cases, the green and red tracks are representative for the medians of the measured total displacements and net displacements in the anteroposterior axis of distant neutrophils and macrophages, respectively. The number of drawn leukocytes at the wound are only representing estimates of the relative numbers in the different genotypes. For the wild type sibling the $tlr2^{+/+}$ sibling was used as an example (A).

basal transcripts for chemokines at the time of wounding is responsible for the observed defects in leukocyte migration behavior. It is also possible that DAMPs released by dead cells around the wound do not lead to secretion of chemokines in the absence of TLR signaling. DAMPs are well known for activating PRRs and then activating downstream chemokines and cytokines secretion [224]. Molecules that can function as DAMPs and associated recognition factors during tissue injury such as hyaluronic acid and HMGB1, have been shown to be directly recognized by TLRs in tissues [268, 229, 269]. Chemokines can be produced by leukocytes which are exposed to reactive oxygen species (ROS) produced by injury [270, 213]. Moreover, previous studies have demonstrated that ROS are required for leukocyte recruitment upon wounding in the zebrafish larval model showing its function in long range chemotaxis to arachidonic acid [251, 254]. It has been demonstrated that the generation of ROS is related to TLR signaling in inflammation and tissue injury [271]. For example, Shishido et al. found that TLR2 mediates the generation of ROS after vascular injury ([272]. Thus, it is possible that the generation of ROS may be decreased in *tlr2* and *myd88* mutant zebrafish larvae.

To study the mechanistic basis of the differences in cell migratory behavior, mathematical and computational models can also provide insights. Chemokine and ROS gradients can easily be modelled by partial differential equations (PDEs). These can also be incorporated into a cell chemotaxis models, such as random walk models, phase field models, or the Cellular Potts model, with varying degrees of cell resolution, to study the chemotaxis of leukocytes. Such models could provide quantitative insights into how chemokine and ROS gradients affect the migration behavior of the leukocytes, and how the cells change these gradients by binding or secretion of chemokines or absorption and metabolizing ROS [273] which is known to affect the robustness of chemotaxis [274]. Using Bayesian inference on tracking data, one can infer a number of chemotaxis parameters, such as the flow rate, diffusion coefficient and production time of the chemoattractant [275]. Furthermore, simulated tracks can be compared to experimentally derived tracks. Altogether, such quantitative approaches in close interaction with new experiments could help demonstrate that the chemokine or ROS gradients are affected by the *tlr2* and *myd88* mutations. For such experiments we will need larger data sets than were currently obtained. This was partially due to the limitations of manual cell tracking. Therefore, in follow-up experiments with larger datasets, the tracking needs to be automated by using automatic tracking algorithms [276, 277, 278]. Currently, the Viterbi algorithm [278] cannot fully track the complex leukocyte cell behaviors: as cell are disappearing and appearing

in the tracking method, this leads to gaps in the time series images. Further optimization of this algorithm can result in the desired quantification of larger data sets.

Better theoretical cell migration analysis methods will also be useful for studying subsequent phases of the inflammatory response after wounding [213]. This can assist us in future studies focused on examining the involvement of the TLR signaling in neutrophil reverse migration and in the repair of wounded tissue. Previously we have reported that *myd88* mutant larvae that were raised under germ-free conditions show increased macrophage and decreased neutrophil numbers in the gut [279]. This indicates that the function of TLR signaling in leukocyte migration is dependent on the gut microbiota. It will be highly interesting to test whether the response of leukocytes to tail wounding is also dependent on the microbiome.

Data Availability Statement

The datasets in present study are available on request to the authors

Ethics Statement

No adult animals were used for experimentation. Larvae for experiments were obtained from zebrafish lines that were handled in compliance with the local animal welfare regulations and maintained according to standard protocols (zfin.org). The breeding of adult fish was approved by the local animal welfare committee (DEC) of the University of Leiden. All protocols adhered to the international guidelines specified by the EU Animal Protection Directive 2010/63/EU for which larvae under the age of 5 days post fertilization are not considered test animals.

Author Contributions

WH performed all biological experiments and manual cell tracking analyses and wrote the first version of the manuscript, LvS performed analyses of cell migration behavior and assisted with statistical analyses, RMHM, FJV and HPS supervised the study, HPS initiated the study and has the final responsibility of the manuscript. All authors delivered input for the final version of the manuscript and agreed with its contents. Chen Li and Lu Cao developed a script and performed automated cell tracking analyses for the published version.

Funding

W.H was supported by grants from the China Scholarship Council (CSC). R.M.H.M was supported by NWO Vici 865.17.004. The funding bodies had no role in the design of the study and collection, analysis, and interpretation of data and in writing the manuscript.

Acknowledgments

We acknowledge Ulrike Nehrdich and Guus van der Velden for the assistance in adult zebrafish care.

Supplementary Material

The supplementary material can be accessed at the site of the publisher.